Optical and Quantum Electronics (2022) 54:222
https://doi.org/10.1007/s11082-022-03597-9

Laser intensity profile based terahertz field enhancement from a mixture of nano-particles embedded in a gas

P. Varshney[1] · A. P. Singh[2] · M. Kundu[1,3] · K. Gopal[2]

Received: 4 October 2021 / Accepted: 17 February 2022 / Published online: 13 March 2022

Abstract
Nano-particle embedded system plays an importance in developing of future terahertz (THz) radiation source for real-world applications. The laser interactions with nanoparticle embedded system can produce a wide range of THz radiation due to plasma oscillations excitation. We investigate THz field generation from the laser-beat wave interaction with a mixture of spherical and cylindrical graphite nanoparticles in argon gas. Different laser intensity distributions such as Gaussian, cosh-Gaussian, flat-top and ring shape laser pulses have been studied in this work. The relevant plasmon resonance conditions with appropriate symmetry of spherical nanoparticles and cylindrical nanoparticles are discussed. THz field is enhanced upto the order of 10^2 when the laser intensity redistributes along the polarization direction for a ring shape field envelope.

Keywords Surface plasmon resonance · Nanoparticles · Terahertz radiation

1 Introduction

Terahertz (THz) radiation lies in between microwave and infrared range of electromagnetic (EM) wave spectrum. It has a number of applications in various areas e.g. medical imaging, terahertz spectroscopy, materials characterization and telecommunications. Conventional sources for THz radiation e.g. optical rectification (Faure et al. 2004), photoconductive antenna (Jepsen et al. 1996), dielectrics (Lan et al. 2017), quantum cascade laser (Szymański et al. 2015) and semiconductors (Hamster et al. 1993) are not efficient enough as emitted radiations are of narrow bandwidth and low efficiency. Laser-plasma interaction can produce highly energetic and ultra-short THz fields. Laser-plasma based methods (Varshney et al. 2015; Varshney et al. 2018; Cho et al. 2015; Gurjar et al. 2020; Singh and Sharma 2013) have been used for high power THz emission in past few years as

✉ K. Gopal
kgopal874u@gmail.com

[1] Institute for Plasma Research, HBNI, Bhat Gandhinagar, Ahmedabad, Gujarat 382428, India

[2] Department of Physics and Electronics, Rajdhani College (University of Delhi), New Delhi, Delhi 110015, India

[3] Homi Bhabha National Institute, Training School Complex, Anushakti nagar, Mumbai 400094, India

plasmas have no damage threshold limit. As laser technology progresses for higher peak intensities (Strickland and Mourou 1985), THz peak power can be increased by scaling up the laser intensity.

Laser induced wakefield comprises electrostatic and electromagnetic components in the presence of a transverse magnetic field. The magnetized wakefield has nonzero group velocity that allows wake to propagate in underdense plasmas and emits electromagnetic radiation at the a plasma-vacuum boundary. THz radiation emits through laser generated wakefield in the presence of a transverse magnetic field in Cherenkov wake radiation mechanism (Yoshii et al. 1997). Amplitude of THz radiation expressed as (ω_c/ω_p) (ratio of electron cyclotron frequency and plasmonic frequency) times the wakefield amplitude. Linear-mode conversion (Sheng et al. 2005b) has been another way to produce THz radiation in non-uniform plasmas, where laser wakefield is converted into electromagnetic radiation with conversion efficiency scaling as $\sim\left(\frac{\omega_T}{\omega_L}\right)^3$, where ω_T and ω_L are the terahertz and laser wave frequency, respectively. Properties of THz radiation can be tuned using the laser intensity and the scale-length of the non-uniform plasmas (Sheng et al. 2005a). Nonlinear mixing of laser beat wave with non-uniform plasmas can generate THz fields under appropriate phase matching conditions (Singh and Sharma 2013; Varshney et al. 2018). THz radiation has also been reported in air and noble gas by using two color lasers (Saxena et al. 2018).

Nanoparticles (NP's) show high-order nonlinearity relative to the collective oscillations of relatively free-electrons at plasmon frequency, which makes NPs a potential candidate for nano-electronic, nano-optic, nano-photonics, and biomedical applications. Heating of the electrons in the NPs array allows coherent THz pulse generation that can be tuned under the variation of the geometries of the metallic NPs (Fadeev et al. 2018). Electron photoemission and ponderomotive acceleration through surface enhanced optical fields can produce THz radiation from gold nano-rods when illuminated by intense laser pulses with different central wavelength (Takano et al. 2019). THz pulses are generated through the acceleration of the ejected electrons under the influence of ponderomotive force that arises from the inhomogeneous plasmon field when femtosecond laser pulses interact with the array of silver nanoparticles. THz emission can be controlled on the basis of metal nanoparticle morphology (Polyushkin et al. 2011). Semiconducting and graphite NPs exhibit collective oscillations at low plasmon frequency in THz range while other metallic NP's have frequency out of the THz range. Therefore, graphite NPs can be explored for the THz radiation generation and related application (Varshney et al. 2020). In the present study, we propose to investigate the induced THz field from the shaped laser beam interaction with a mixture of NPs in Argon gas (see schematics in Fig. 1). Shape of the NPs can be tailored to tune the plasmon frequency and therefore, the properties of the THz field. Different types of laser intensity profiles have been employed to enhance the THz field from nano-particle interaction.

This work is based on the laser intensity profile effect on THz field generation via nano-particle dynamics. The laser intensity distribution is varied for different laser electric field profile (see in Fig. 2). Previously (Sharma et al. 2020), THz field generation has reported from mixture of nanoparticles where they used same resonance condition for spherical and cylindrical nanoparticles (with same plasma frequency of electron dynamics) that is inappropriate to consider for the estimation of THz field. We consider different plasmon resonance conditions for different shapes of the nanoparticles. Different restoring forces for both spherical and cylindrical NPs that lead to different plasmon resonance conditions have been considered for accurate THz field estimation. Energy

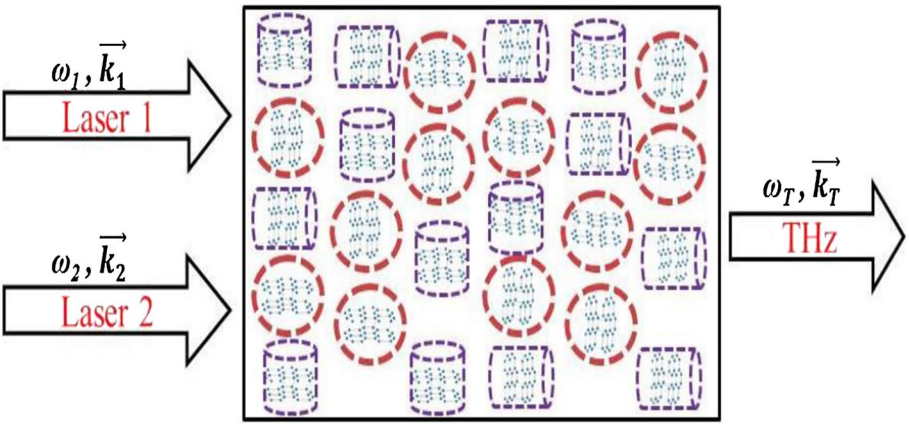

Fig. 1 Schematic representation of THz field generation from laser beat-wave interaction with nanoparticle embedded argon gas

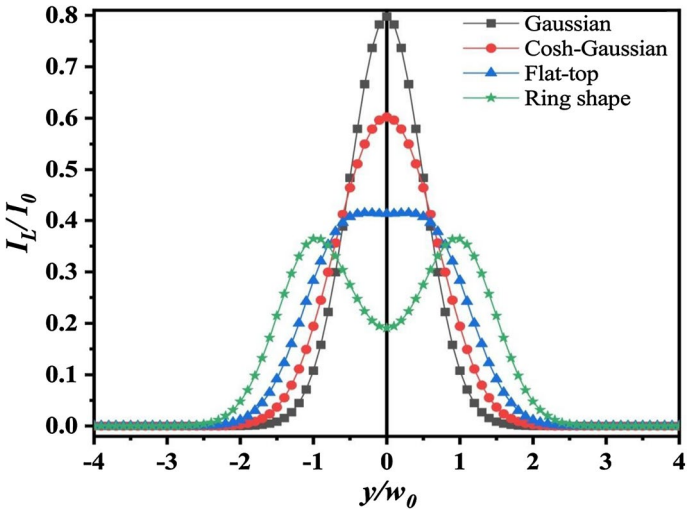

Fig. 2 Intensity distribution corresponding to laser field profile for Gaussian *(black)*, Cosh Gaussian (*red*), Flat-top Gaussian (blue) and Ring shape (green) pulses. (Color figure online)

loss mechanism has also been considered in this formulation with a damping factor (Γ). Contribution of the non-conducting and the bound electron of the background is being included in the calculations of the effective permittivity. Here, THz field has been estimated and discussed for varying shape of laser field envelope, basal plane spacing and laser spot size. Finally, results are summarized in the last Sec. In present study, we have considered the redistribution of laser intensity considering the field profile that has beam decentred parameter; this parameter allows the intensity redistribution in space. Therefore, we are reporting beam decentred parameter as a controlling knob for THz field.

2 Physical model and THz field calculation

We consider the nonlinear mixing of lasers in plasma embedded by nanoparticles for emission of THz radiation. Schematic of the physical mechanism is shown in Fig. 1. We consider two linearly polarized cosh-Gaussian laser pulses co-propagating through a mixture of NPs in argon gas. Electric field profile corresponding to the laser pulses is defined as (Lü et al. 1999; Mei and Korotkova 2013)

$$\vec{E}_j = \hat{y}\, E_0 \cosh\left(\frac{yb}{w_0}\right) e^{-y^2/w_0^2} e^{-i(\omega_j t - k_j z)}, \tag{1}$$

where $j = 1, 2$ represents two different lasers, w_0 is the laser beam-width, E_0 is the laser electric field amplitude. Variation in the parameter (b) changes the field envelope of the laser e.g. Gaussian beam (b=*0*), Cosh Gaussian (b=*1*), flat-top Gaussian (b=*1.45*) and ring shape (b=*2*). Intensity redistribution related to the above mentioned field profile of lasers is shown in Fig. 2. Laser intensity is estimated using the average value laser electric field as $\epsilon_0 \langle E_{avg}^2 \rangle / 2$. Here, we consider the geometries of spherical and cylindrical geometries of NPs with their basal plane (plane perpendicular to the principal axis in the crystal systems) oriented in two different directions, i.e., normal to the electric field $\vec{E}_j || k_{i(=z)}$ and parallel to the electric field $\vec{E}_j \perp k_{i(=y)}$, where k_i is the symmetry axis normal to the basal plane with different orientations within the nanoparticle.

Since the mixture of SNPs and CNPs is considered in host Ar gas, the total macroscopic density of nanoparticles is expressed as (Sharma et al. 2020)

$$n_0 = \sum_{k_i} (n_s + n_c) = \sum_{k_i} n_{0,k_i} (g_{sk_i} + g_{ck_i}), \tag{2}$$

Where n_s and n_c represents the densities of SNPs and CNPs, respectively. Particle anisotropy is an important factor that leads to self-assembly of NPs in a specific shape. Experimentally, wet chemical methods have been used widely for production of spherical and cylindrical metal nanoparticles (Sharma et al. 2020; Guerrero-Martínez 2011). The factors $g_{sk_i} = 4\pi r_{sk_i}^3 / 3 d_{sk_i}^3$ and $g_{ck_i} = \pi r_{ck_i}^2 h_{ck_i} / d_{ck_i}^3$ represent the volume fraction, i.e. the volume occupied by SNPs and CNPs divided by volume of the unit cell for each of the directions (perpendicular and parallel), where d_{sk_i}, d_{ck_i} and r_{sk_i}, r_{ck_i} are the average distance and radii between two consecutive cylindrical nanoparticles and spherical nanoparticles in a given direction, respectively.

Here, we are assuming that charges are distributed evenly around the nanoparticles and the modulated density of CNPs and SNPs can be written as

$$n' = n_\alpha\, e^{i\alpha z}, \tag{3}$$

where n_α and α are the amplitude and the wave number of the density ripples.

Density modulation of nanoparticles in the above mentioned pattern can be produced with the stream of nanoparticles through nozzle in the background host Ar gas. The motion of spherical and cylindrical electron clouds corresponding to NPs can be compared with the motion of a single electron in a laser electric field. Therefore, nonrelativistic electron cloud dynamics can be expressed in the form of an electron's equation of motion as (Varshney et al. 2020)

$$\frac{d\overrightarrow{v_j}}{dt} + \delta_{Gen}\overrightarrow{x_j} + \Gamma\overrightarrow{v_j} = -\frac{e}{m}\overrightarrow{E_j}, \tag{4}$$

where m is the mass of electron, e is the electron charge, Γ is the damping factor and $\omega_p = \left(4\pi n_0 e^2/m\right)^{1/2}$ is electron plasma frequency. Damping mechanisms during laser beat wave interaction with clustered plasma include electron-electron, electron-phonon and electron-surface scattering. The term $\delta_{Gen}x_j$ represents the generalised restoring force exerted by immobile ions, which helps to return the electronic cloud to its equilibrium state in the presence of a laser electric field. For the spherical nanoparticles $\delta_{Gen} = \delta_{sp} = \omega_p^2/3$, the cylindrical nanoparticles oriented with perpendicular direction of wave propagation $\delta_{Gen} = \delta_{cy\perp} = \omega_p^2/2$ and cylindrical nanoparticles oriented with parallel direction of wave propagation $\delta_{Gen} = \delta_{cy||} = \omega_p^2$. Oscillatory velocity for the electrons can obtained from Eq. (4) as

$$\overrightarrow{v_j} = \frac{-ie\omega_j\overrightarrow{E_j}}{m(\omega_j^2 + i\Gamma\omega_j - \delta_{Gen})}, \tag{5}$$

The ponderomotive force ($\vec{F}_{NL}$) is a non-linear force that imparts on conduction electrons at the beat frequency $\omega = \omega_1 - \omega_2$ by the inhomogeneous electric field of laser beat wave. Ponderomotive force can be estimated using the standard formulation of ponderomotive potential $\phi_p = -m\,\vec{v}_1 * \vec{v}_2^*/2\,e$ as (Varshney et al. 2020)

$$\overrightarrow{F_p^{NL}} = \frac{-e^2\omega_1\omega_2E_0^2}{2m} * \frac{\left\{-\frac{2y}{w_0^2} + \frac{b}{w_0}\sinh\left(\frac{2yb}{w_0}\right) - \frac{2y}{w_0^2}cosh\left(\frac{2yb}{w_0}\right)\hat{y} - ik'\hat{z}\right\}\exp[-2y^2/w_0^2] * \exp[i(k'z - \omega t)]}{(\omega_1^2 + i\Gamma\omega_1 - \delta_{Gen})(\omega_2^2 + i\Gamma\omega_2 - \delta_{Gen})} \tag{6}$$

Further, one can write equation of motion under the effect of ponderomotive force as

$$\frac{\partial^2\overrightarrow{x^{NL}}}{\partial t^2} + \delta_{Gen}\overrightarrow{x^{NL}} + \Gamma\frac{\partial\overrightarrow{x^{NL}}}{\partial t} = \frac{\overrightarrow{F_p^{NL}}}{m}, \tag{7}$$

where $\vec{x}^{NL}$ is the displacement of the electrons. Y-component of the nonlinear velocity $\vec{v}^{NL}$ of the electrons can be obtained by solving Eq. (7) as

$$v_y^{NL} = \frac{ie^2\omega_1\omega_2\omega E_0^2}{2m^2} * \frac{\left\{-\frac{2y}{w_0^2} + \frac{b}{w_0}\sinh\left(\frac{2yb}{w_0}\right) - \frac{2y}{w_0^2}cosh\left(\frac{2yb}{w_0}\right)\right\}\exp[-2y^2/w_0^2] * \exp[i(k'z - \omega t)]}{(\omega^2 + i\Gamma\omega - \delta_{Gen})(\omega_1^2 + i\Gamma\omega_1 - \delta_{Gen})(\omega_2^2 + i\Gamma\omega_2 - \delta_{Gen})} \tag{8}$$

Hence the nonlinear macroscopic current density is evaluated by taking the contribution of both types of oriented NPs as

$$J_y^{NL} = \sum_{k_i}(\delta_1 * g_{sk_i} + \delta_2 * g_{ck_{i\perp}} + \delta_3 * g_{ck_{i\parallel}})n'ev_y^{NL}, \tag{9}$$

where δ_1, δ_2 & δ_3 are the arbitrary constants considered to include the individual contribution of spherical, cylindrical and mixture of spherical & cylindrical nanoparticles.

$$\left(J_y^{NL}\right) = \frac{ie^3\omega_1\omega_2\omega n_\alpha E_0^2}{2m^2} * \exp[i\{(k'+\alpha)z-\omega t)] * \left\{-\frac{2y}{w_0^2}+\frac{b}{w_0}\sinh\left(\frac{2yb}{w_0}\right)-\frac{2y}{w_0^2}cosh\left(\frac{2yb}{w_0}\right)\right\}\exp\left[\frac{-2y^2}{w_0^2}\right] * \left\{\begin{array}{l}\frac{\delta_1\left(\frac{-4\pi r_{sk_i}^3}{3d_{sk_i}^3}\right)}{(\omega^2+i\Gamma\omega-\omega_P^2/3)(\omega_1^2+i\Gamma\omega_1-\omega_P^2/3)(\omega_2^2+i\Gamma\omega_2-\omega_P^2/3)}+ \\ \frac{-\pi r_{ck_i}^2 h_{ck_i}}{d_{ck_i}^3} * \left\{\begin{array}{l}\frac{\delta_2}{(\omega^2+i\Gamma\omega-\omega_P^2/2)(\omega_1^2+i\Gamma\omega_1-\omega_P^2/2)(\omega_2^2+i\Gamma\omega_2-\omega_P^2/2)} \\ +\frac{\delta_3}{(\omega^2+i\Gamma\omega-\omega_P^2)(\omega_1^2+i\Gamma\omega_1-\omega_P^2)(\omega_2^2+i\Gamma\omega_2-\omega_P^2)}\end{array}\right.\end{array}\right. \tag{10}$$

SNPs follow radial symmetry, while CNPs have cylindrical symmetry. Therefore, CNPs are considered to be oriented in parallel and perpendicular to the laser polarization. Expression for nonlinear current density can be estimated using Eqs. (8) and (9) and described in Eq. (10).

The THz field wave equation is obtained from Maxwell's equations, as given below

$$\nabla^2\vec{E}_{THz} - \vec{\nabla}.\left(\vec{\nabla}.\vec{E}_{THz}\right) + \frac{\omega^2}{c^2}\left(\varepsilon_{eff}.\vec{E}_{THz}\right) = -\frac{4\pi i\omega}{c^2}\vec{J}^{NL}, \tag{11}$$

where ε_{eff} is the effective electric permittivity tensor of the medium of cylindrical and spherical graphite nanoparticles. Majorly, the conduction electrons of the graphite NPs give rise to nonlinearity. Effective permittivity of the medium needs to be calculated that consider both conducting and non-conducting bound electrons of the medium and, therefore, mathematical expression for the effective permittivity can be written as(Sau and Rogach 2012)

$$\left(\varepsilon_{eff}\right)_{Gen} = \varepsilon_i^b + \varepsilon^f = \varepsilon_i^b + 1 - \frac{\omega_p^2}{(\omega^2+i\Gamma\omega-\delta_{Gen})} \tag{12}$$

Since it contains two separate shapes of graphite nanoparticles of different orientations, the efficient permittivity of the host medium is altered. Due to the introduction of SNPs and CNPs, the contribution of bound electrons to efficient permittivity can be rewritten as $\varepsilon_i^b = \varepsilon(s) + \varepsilon(c)/2$, where

$$\varepsilon(s) = \varepsilon_h + 3\varepsilon_h\frac{\sum_{k_i} g_{sk_i}\frac{\varepsilon_{k_i}-\varepsilon_h}{\varepsilon_{k_i}+2\varepsilon_h}}{1-\sum_{k_i} g_{sk_i}\frac{\varepsilon_{k_i}-\varepsilon_h}{\varepsilon_{k_i}+2\varepsilon_h}}, \tag{13}$$

$$\varepsilon(c) = \varepsilon_h + \sum_{k_i} g_{ck_i} \frac{(\varepsilon_{k_i} - \varepsilon_h)(\varepsilon_{k_i} + 5\varepsilon_h)}{(3 - 2g_{ck_i})\varepsilon_{k_i} + (3 + 2g_{ck_i})\varepsilon_h}, \tag{14}$$

where ε_h is the permittivity of host medium and ε_{k_i} is the permittivity of bound electrons (only) for different orientations of nanoparticles.

Expression for the THz field can be obtained taking the divergence of Eq. (11) and considering the assumption $\upsilon^2 < \omega^2$

$$\vec{E}_{THz} = -\frac{4\pi i}{\omega \varepsilon_{eff}} \vec{J}^{NL} \tag{15}$$

Substituting Eq. (10) into Eq. (15), one can obtain the expression for the normalized THz radiation fields under consideration of only spherical nanoparticles ($\delta_1 = 1,\ \&\ \delta_2 = \delta_3 = 0$), only cylindrical nanoparticles ($\delta_1 = 0,\ \&\ \delta_2 = \delta_3 = 1$), and the mixture of spherical and cylindrical nanoparticles ($\delta_1 = \delta_2 = \delta_3 = 1$):

$$\left|\frac{E_{THz}}{E_0}\right| = \frac{e\omega_1\omega_2 n_\alpha E_0 \omega_p^2}{2mn_0} * \left\{ -\frac{2y}{w_0^2} + \frac{b}{w_0} \sinh\left(\frac{2yb}{w_0}\right) - \frac{2y}{w_0^2} cosh\left(\frac{2yb}{w_0}\right) \right\} * \exp\left[\frac{-2y^2}{w_0^2}\right] *$$
$$\left(\delta_1 * \left\{ \frac{4\pi r_{sk_i}^3}{3d_{sk_i}^3} * \frac{1}{(\varepsilon_{eff})_{sp}} * \frac{1}{\left(\omega^2 + i\Gamma\omega - \frac{\omega_p^2}{3}\right)\left(\omega_1^2 + i\Gamma\omega_1 - \frac{\omega_p^2}{3}\right)\left(\omega_2^2 + i\Gamma\omega_2 - \frac{\omega_p^2}{3}\right)} \right\} \right.$$
$$+\delta_2 * \left\{ \frac{\pi r_{ck_i}^2 h_{ck_i}}{d_{ck_i}^3} * \frac{1}{(\varepsilon_{eff})_{cy\parallel}} * \frac{1}{\left(\omega^2 + i\Gamma\omega - \frac{\omega_p^2}{2}\right)\left(\omega_1^2 + i\Gamma\omega_1 - \frac{\omega_p^2}{2}\right)\left(\omega_2^2 + i\Gamma\omega_2 - \frac{\omega_p^2}{2}\right)} \right\}$$
$$\left. +\delta_3 * \left\{ \frac{\pi r_{ck_i}^2 h_{ck_i}}{d_{ck_i}^3} * \frac{1}{(\varepsilon_{eff})_{cy\perp}} * \frac{1}{\left(\omega^2 + i\Gamma\omega - \omega_p^2\right)\left(\omega_1^2 + i\Gamma\omega_1 - \omega_p^2\right)\left(\omega_2^2 + i\Gamma\omega_2 - \omega_p^2\right)} \right\} \right) \tag{16}$$

Number density of the embedded nanoparticles has been considered same while estimating the normalised THz field amplitude in Eq. (16). The efficiency of the THz radiation generation can be estimated by calculating the ratio of the energies of THz radiation to the incident laser (pump). Conversion efficiency of the THz emission in present physical mechanism can be expressed as $\eta = W_{THz}/W_{pump}$, where the average energy densities of the emitted radiation W_{THz} and the incident pump lasers W_{pump} are ,

$$W_{pump} = \sqrt{\frac{\pi}{2}} \frac{\varepsilon_0 E_0^2}{2} \frac{1}{\sqrt{\frac{1}{w_0^2}}} (1 + e^{b^2/2}) \tag{17}$$

$$W_{THz} = \frac{\varepsilon_0 E_0^2}{2}\sqrt{\frac{\pi}{2}} * \left(\frac{n_\alpha}{n_0}\right)^2 \frac{e^2\omega_1^2\omega_2^2\omega_p^4}{4m^2}\left[\frac{3-b^2+4e^{b^2/2}+(1+b^2)e^{2b^2}}{2*\left(1/w_0^2\right)^{3/2} w_0^4}\right]*$$
$$\left(\begin{array}{l}\left\{\frac{4\pi r_{sk_i}^3}{3d_{sk_i}^3} * \frac{1}{(\varepsilon_{eff})_{sp}} * \frac{\delta_1}{\left(\omega^2+i\Gamma\omega-\frac{\omega_p^2}{3}\right)\left(\omega_1^2+i\Gamma\omega_1-\frac{\omega_p^2}{3}\right)\left(\omega_2^2+i\Gamma\omega_2-\frac{\omega_p^2}{3}\right)}\right\} \\ +\left\{\frac{\pi r_{ck_i}^2 h_{ck_i}}{d_{ck_i}^3} * \frac{1}{(\varepsilon_{eff})_{cy\|}} * \frac{\delta_2}{\left(\omega^2+i\Gamma\omega-\frac{\omega_p^2}{2}\right)\left(\omega_1^2+i\Gamma\omega_1-\frac{\omega_p^2}{2}\right)\left(\omega_2^2+i\Gamma\omega_2-\frac{\omega_p^2}{2}\right)}\right\} \\ +\left\{\frac{\pi r_{ck_i}^2 h_{ck_i}}{d_{ck_i}^3} * \frac{1}{(\varepsilon_{eff})_{cy\perp}} * \frac{\delta_3}{\left(\omega^2+i\Gamma\omega-\omega_p^2\right)\left(\omega_1^2+i\Gamma\omega_1-\omega_p^2\right)\left(\omega_2^2+i\Gamma\omega_2-\omega_p^2\right)}\right\}\end{array}\right)^2 \tag{18}$$

Equation (19) describes the efficiency of THz radiation fields under consideration for three different cases (i) only spherical nanoparticles ($\delta_1 = 1,\ \&\ \delta_2 = \delta_3 = 0$) (ii) only cylindrical nanoparticles ($\delta_1 = 0,\ \&\ \delta_2 = \delta_3 = 1$), and (iii) the mixture of SNPs and CNPs ($\delta_1 = \delta_2 = \delta_3 = 1$).

$$\eta = \left(\frac{n_\alpha}{n_0}\right)^2 \frac{e^2\omega_1^2\omega_2^2\omega_p^4}{8m^2}\left[\frac{3-b^2+4e^{b^2/2}+(1+b^2)e^{2b^2}}{(1+e^{b^2/2})w_0^2}\right]*$$
$$\left(\begin{array}{l}\left\{\frac{4\pi r_{sk_i}^3}{3d_{sk_i}^3} * \frac{1}{(\varepsilon_{eff})_{sp}} * \frac{\delta_1}{\left(\omega^2+i\Gamma\omega-\frac{\omega_p^2}{3}\right)\left(\omega_1^2+i\Gamma\omega_1-\frac{\omega_p^2}{3}\right)\left(\omega_2^2+i\Gamma\omega_2-\frac{\omega_p^2}{3}\right)}\right\} \\ +\left\{\frac{\pi r_{ck_i}^2 h_{ck_i}}{d_{ck_i}^3} * \frac{1}{(\varepsilon_{eff})_{cy\|}} * \frac{\delta_2}{\left(\omega^2+i\Gamma\omega-\frac{\omega_p^2}{2}\right)\left(\omega_1^2+i\Gamma\omega_1-\frac{\omega_p^2}{2}\right)\left(\omega_2^2+i\Gamma\omega_2-\frac{\omega_p^2}{2}\right)}\right\} \\ +\left\{\frac{\pi r_{ck_i}^2 h_{ck_i}}{d_{ck_i}^3} * \frac{1}{(\varepsilon_{eff})_{cy\perp}} * \frac{\delta_3}{\left(\omega^2+i\Gamma\omega-\omega_p^2\right)\left(\omega_1^2+i\Gamma\omega_1-\omega_p^2\right)\left(\omega_2^2+i\Gamma\omega_2-\omega_p^2\right)}\right\}\end{array}\right)^2 \tag{19}$$

3 Result and discussion

This section describes the numerical results obtained from the physical model for THz field generation using nonlinear mixing phenomena, where laser beat wave envelope interacts with the density modulated mixture of SNPs and CNPs. Laser intensity redistribution along the polarization direction affects the ponderomotive force strongly that influences the nonlinear transverse current. Since transverse current is a key source for radiation generation, laser intensity redistribution is treated as a significant parameter in present numerical calculations to estimate the properties of THz radiations. THz field amplitude has been estimated as a function of THz frequency for variation in laser intensity distribution under

different spatial field envelopes e.g. Gaussian, cosh-Gaussian, flat-Gaussian and ring shape. In present numerical calculations, we have considered CO_2 laser with frequency $\omega_1 = 2 \times 10^{14} rad/sec\left(\lambda_l = 10.1\mu m\right)$, intensity $I = 2 \times 10^{15} w/cm^2$ and spot size of $10\mu m$,$20\mu m$,$30\mu m$, and $40\mu m$ respectively. Plasma frequency has been chosen as $\omega_p = 2\pi \times 10^{12} rad/sec$ corresponding to the plasma density $n_0 = 1.24 \times 10^{16} cm^{-3}$. Density modulation is considered as 30% of the background plasma density for individual NPs and mixture of NPs. Oscillatory velocity of electrons corresponding to above mentioned laser intensity is $v_1 = 0.3c$. Number density of embedded NPs is the same while considering individual SNPs, CNPs or the mixture of NPs. Aspect ratio (height to width) is considered unity in present set of numerical calculations for CNPs. Transverse nonlinear current is the key source for the generation of THz field in laser-plasma based methods. Fig. 3 shows the normalised THz amplitude as function of normalised frequency for spatially varying laser field envelope in case of SNPs, CNPs, and the mixture of SNPs and CNPs respectively. THz field attains peak value when laser beat frequency ($\omega = \omega_1 - \omega_2$) approaches the resonance. Plasmon oscillations resonates at the surface of SNPs when $\omega_1 - \omega_2 = \frac{\omega_p}{\sqrt{3}}$, while resonance arises at $\omega_1 - \omega_2 = \frac{\omega_p}{\sqrt{2}}$ and $\omega_1 - \omega_2 = \omega_p$ for CNPs in parallel and perpendicular orientation with laser propagation direction. The THz field decreases as one move away from the resonance.

Exact phase matching and resonant excitation of THz radiation is achieved by introducing density modulation with suitable ripple wave number. Exact matching of the ripple wave vector with the laser beat wave number provides the maximum transfer of energy and momentum for resonance conditions. Previously (Sharma et al. 2020), THz field estimated considering the same plasmon resonance condition for both SNPs and CNPs that is inappropriate to consider as the plasmon resonance condition depends on the symmetry of NPs. From Fig. 3(b), it is observed that CNPs contribute more towards the THz field in comparison to the SNPs, where the radius of both the NPs and the basal plane spacing is considered the same. Also, the resonance appears to shift (in Figs. 3(a) and (b)) towards the higher value of frequency in case of CNPs that indicate the variation in timescale of effective energy transfer from laser beat wave to CNPs in comparison to SNPs. Nonlinear current density enhances as the number of conduction electrons per unit volume increases for mixture of SPNs and CNPs. Therefore, the mixture of the SNPs and CNPs contributes more toward the THz field as shown in Fig. 3(c). Here, variation in laser intensity distribution greatly affects the nonlinear current density as ponderomotive force enhances when laser intensity re-distributed along the polarization direction and therefore, THz field increases for ring shape field envelope. Twofold enhancement in THz field amplitude observed in case of ring shape laser field envelope for mixture of SNPs and CNPs in comparison to numerical results reported previously (Javan et al. 2017), where density modulated SNPs are embedded in argon gas for THz field generation. Recently (Varshney et al. 2022), THz field of the order $\approx 10^{-6}$ reported using nonlinear mixing of laser pulses in semiconductor plasmas that is less than the THz field reported in present study. Therefore, mixture of nanoparticles embedded in argon gas produces better THz field as a source medium in comparison to semiconductor plasmas.

Since the graphite NPs are anisotropic in nature, orientation of the basal plane and related spacing is the key factor to consider in present numerical calculations. Basal plane spacing can also affect the THz field amplitude as number density of NPs varies with basal plane spacing $(d_s) or (d_c)$. Therefore, the number of conduction electrons of the spherical and cylindrical cloud of electrons involved in plasmon excitation vary that would change the transverse nonlinear current. Fig. 4 shows the variation of THz field with basal plane

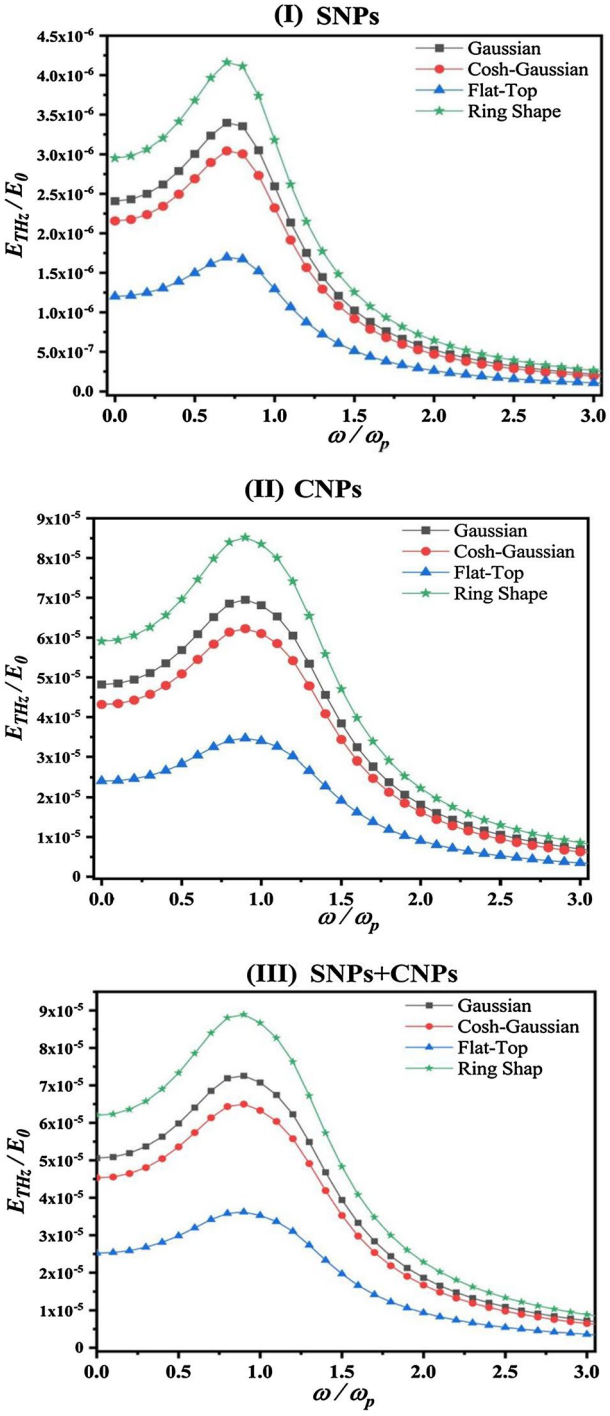

Fig. 3 Normalised THz amplitude $\left(E_{THz}/E_0\right)$ with normalised terahertz frequency (ω/ω_p) for shaped laser pulses (I) SNPs (II) CNPs (III) Mixture of SNPs and CNPs. Laser-plasma parameter considered with frequency $\omega_1 = 2\times10^{14} rad/sec\left(\lambda_l = 10.1\mu m\right)$, intensity $I = 2\times10^{15} w/cm^2$, plasma frequency $\omega_p = 2\pi\times10^{12} rad/sec$ corresponding to the plasma density $n_0 = 1.24\times10^{16} cm^{-3}$

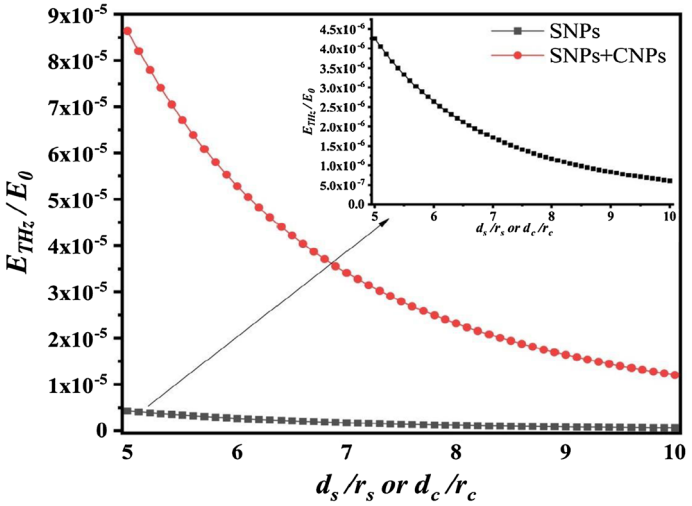

Fig. 4 Normalised THz amplitude $\left(E_{THz}/E_0\right)$ as function of basal plane spacing for spherical, cylindrical and combination of spherical and cylindrical nanoparticles in case of ring shape field envelope. Laser-plasma parameter considered with frequency $\omega_1 = 2\times10^{14} rad/sec\left(\lambda_l = 10.1\mu m\right)$, intensity $I = 2\times10^{15} w/cm^2$, Plasma frequency $\omega_p = 2\pi\times10^{12} rad/sec$ corresponding to plasma density $n_0 = 1.24\times10^{16} cm^{-3}$

spacing for ring shape laser field envelope in case of only SNPs and mixture of NPs (SNPs & CNPs). THz field decreases for increasing value of basal plane spacing.

Figure 5 show the THz field as a function of normalised frequency for varying laser beam width parameter. Ponderomotive force increases for smaller beam width as laser

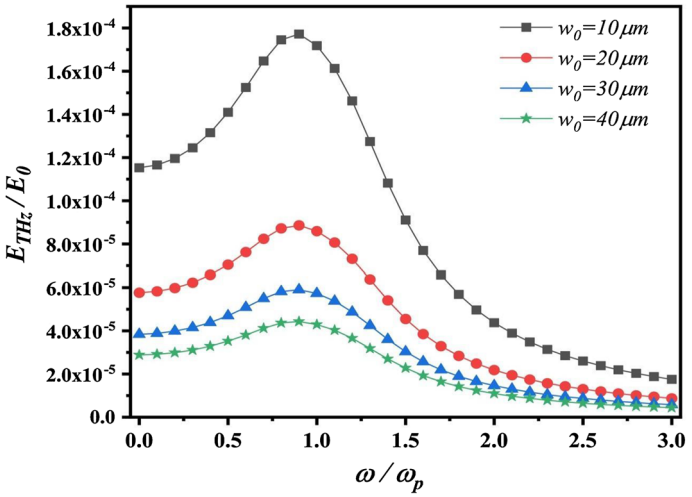

Fig. 5 Normalised THz amplitude $\left(E_{THz}/E_0\right)$ as function of normalized terahertz frequency (ω/ω_p) and laser beam width corresponding to ring shape field envelope. Laser-plasma parameter considered with frequency $\omega_1 = 2\times10^{14} rad/sec\left(\lambda_l = 10.1\mu m\right)$, intensity $I = 2\times10^{15} w/cm^2$, Plasma frequency $\omega_p = 2\pi\times10^{12} rad/sec$ corresponding to plasma density $n_0 = 1.24\times10^{16} cm^{-3}$

intensity is distributed in a small area that leads to maximum laser energy transfer to the NPs and hence there excite large amplitude surface plasmon. Therefore, nonlinear current density increases and hence THz amplitude enhances for decreasing value of the laser beam width.

Efficiency (η) for the present physical mechanism of THz emission has been derived in the physical model (see Eq. 19). Conversion efficiency of the order 10^{-12} estimated for spherical NPs in case of Gaussian pulses while it enhanced significantly and estimated as 10^{-6} for a mixture of spherical and cylindrical NPs using ring shape laser pulses. Laser energy transfers efficiently in THz field when intensity distribution is changing from Gaussian field envelope to ring shaped field envelope. Ponderomotive force changes significantly when laser intensity spread spatially. Here, we also estimated theoretically the power and energy of emitted THz radiation as 10^3 *Watt* and 5 n Joule for incident laser pulse of 10^8 *Watt* and energy of 10 mJ.

4 Conclusion

Laser intensity distribution plays a significant role in tuning the THz field generated from the laser beat wave interaction with a mixture of nanoparticles (Spherical and cylindrical) in argon gas. Plasmon resonance condition depends on the symmetry of the NPs. Therefore, surface plasmon resonates when $\omega_1 - \omega_2 = \frac{\omega_p}{\sqrt{3}}$ for SNPs, $\omega_1 - \omega_2 = \frac{\omega_p}{\sqrt{2}}$ and $\omega_1 - \omega_2 = \omega_p$ for CNPs in different orientations with the laser propagation direction. Nonlinear transverse current increases as laser intensity redistributes spatially. THz field attains peak value when laser beat frequency ($\omega_1 - \omega_2$) approaches the resonance. Basal plane spacing and laser spot size also affects the THz field significantly. Present study concludes that a ring shape electric field envelope produces a higher THz field in comparison to the Gaussian, flat Gaussian and Cosh-Gaussian field envelope being used with the mixture of SNPs and CNPs in Ar gas.

Acknowledgement The authors would like to thank Prof DN Gupta (Delhi University) for careful reading of the manuscript and providing the useful suggestions. Also, the Author (K Gopal) dedicates this paper to his late friend Dr. Tarun Choudhary, Assistant Profesor Daulat Ram College, University of Delhi-110007 India, who lost his life battling the pandemic situation of covid-19 during academic duties.

Funding One of the authors P. Varshney acknowledges the Institute for Plasma Research Gandhinagar-382428, Gujarat, India for providing financial support to carry out his post Ph.D. research work.

Data availability The data that support the findings of this study are available from the corresponding author upon reasonable request.

Declarations

Conflict of interest We declare that we do not have any commercial or associative interest that represents a conflict of interest in connection with the work submitted.

References

Cho, M.H., Kim, Y.K., Suk, H., Ersfeld, B., Jaroszynski, D.A., Hur, M.S.: Strong terahertz emission from electromagnetic diffusion near cutoff in plasma. New J. Phys. **17**, 043045 (2015). https://doi.org/10.1088/1367-2630/17/4/043045

Fadeev, D.A., Oladyshkin, I.V., Mironov, V.A.: Terahertz emission from metal nanoparticle array. Opt. Lett. **43**, 1939–1942 (2018). https://doi.org/10.1364/ol.43.001939

Faure, J., Van Tilborg, J., Kaindl, R.A., Leemans, W.P.: Modelling laser-based table-top thz sources: optical rectification, propagation and electro-optic sampling. Opt. Quant. Electron. **36**, 681–697 (2004). https://doi.org/10.1023/B:OQEL.0000039617.85129.c2

Guerrero-Martínez, A.: Nanostars shine bright for you Colloidal synthesis, properties and applications of branched metallic nanoparticles. Current Opin. Colloid Interface Sci. **16**, 118–127 (2011). https://doi.org/10.1016/j.cocis.2010.12.007

Gurjar, M.C., Gopal, K., Gupta, D.N., Kulagin, V.V., Suk, H.: High-field coherent terahertz radiation generation from chirped laser pulse interaction with plasmas. IEEE Trans. Plasma Sci. **48**, 3727–3734 (2020). https://doi.org/10.1109/tps.2020.3022903

Hamster, H., Sullivan, A., Gordon, S., White, W., Falcone, R.W.: Subpicosecond, electromagnetic pulses from intense laser-plasma interaction. Phys. Rev. Lett. **71**, 2725–2728 (1993). https://doi.org/10.1103/PhysRevLett.71.2725

Javan, N.S., Erdi, F.R.: Theoretical study of the generation of terahertz radiation by the interaction of two laser beams with graphite nanoparticles. J. Appl. Phys. **122**, 223103 (2017). https://doi.org/10.1063/1.4995510

Jepsen, P.U., Jacobsen, R.H., Keiding, S.R.: Generation and detection of terahertz pulses from biased semiconductor antennas. J. Opt. Soc. Am. B **13**, 2424–2436 (1996). https://doi.org/10.1364/josab.13.002424

Lan, C., Bi, K., Li, B., Zhao, Y., Qu, Z.: Flexible all-dielectric metamaterials in terahertz range based on ceramic microsphere/PDMS composite. Opt. Express **25**, 29155–29160 (2017). https://doi.org/10.1364/oe.25.029155

Lü, B., Ma, H., Zhang, B.: Propagation properties of cosh-Gaussian beams. Opt. Commun. **164**, 165–170 (1999)

Mei, Z., Korotkova, O.: Cosine-Gaussian Schell-model sources. Opt. Lett. **38**, 2578–2580 (2013). https://doi.org/10.1364/ol.38.002578

Polyushkin, D.K., Hendry, E., Stone, E.K., Barnes, W.L.: THz generation from plasmonic nanoparticle arrays. Nano Lett. **11**, 4718–4724 (2011). https://doi.org/10.1021/nl202428g

Sau, T.K., Rogach, A.L.: Complex-shaped metal nanoparticles. John Wiley and Sons, Hoboken (2012)

Saxena, S., Bagchi, S., Rao, B.S., Naik, P.A., Chakera, J.A.: Single-shot terahertz time profiling using curved wavefront. IEEE Trans. Terahertz Sci. Technol. **8**, 528–534 (2018). https://doi.org/10.1109/tthz.2018.2851154

Sharma, D., Singh, D., Malik, H.K.: Shape-dependent terahertz radiation generation through nanoparticles. Plasmonics **15**, 177–187 (2020). https://doi.org/10.1007/s11468-019-01017-5

Sheng, Z.-M., Mima, K., Zhang, J.: Powerful terahertz emission from laser wake fields excited in inhomogeneous plasmas. Phys. Plasm. **12**, 123103 (2005a). https://doi.org/10.1063/1.2136107

Sheng, Z.-M., Mima, K., Zhang, J., Sanuki, H.: Emission of electromagnetic pulses from laser wakefields through linear mode conversion. Phys. Rev. Lett. **94**, 095003 (2005b). https://doi.org/10.1103/PhysRevLett.94.095003

Singh, M., Sharma, R.P.: Generation of THz radiation by laser plasma interaction. Contrib. Plasma Phys. **53**, 540–548 (2013). https://doi.org/10.1002/ctpp.201300006

Strickland, D., Mourou, G.: Compression of amplified chirped optical pulses. Opt. Commun. **55**, 447–449 (1985). https://doi.org/10.1016/0030-4018(85)90151-8

Szymański, M., Szerling, A., Kosiel, K.: Theoretical investigation of metal–metal waveguides for terahertz quantum-cascade lasers. Opt. Quant. Electron. **47**, 843–849 (2015). https://doi.org/10.1007/s11082-014-0007-z

Takano, K., Asai, M., Kato, K., Komiyama, H., Yamaguchi, A., Iyoda, T., Tadokoro, Y., Nakajima, M., Bakunov, M.I.: Terahertz emission from gold nanorods irradiated by ultrashort laser pulses of different wavelengths. Sci. Rep. **9**, 3280 (2019). https://doi.org/10.1038/s41598-019-39604-5

Varshney, P., Gopal, K., Upadhyay, A.: Terahertz emission from nonlinear interaction of laser beat wave with nanoparticles. Laser Phys. Lett. **17**, 126002 (2020). https://doi.org/10.1088/1612-202x/abbeea

Varshney, P., Sajal, V., Singh, K.P., Kumar, R., Sharma, N.K.: Tunable and efficient terahertz radiation generation by photomixing of two super Gaussian laser pulses in a corrugated magnetized plasma. J. Appl. Phys. **117**, 193303 (2015). https://doi.org/10.1063/1.4921357

Varshney, P., Singh, A.P., Upadhyaay, A., Kundu, M., Gopal, K.: Effect of laser intensity redistribution on semiconductor plasma based THz emission. Optik **250**, 168353 (2022). https://doi.org/10.1016/j.ijleo.2021.168353

Varshney, P., Upadhayay, A., Madhubabu, K., Sajal, V., Chakera, J.A.: Strong terahertz radiation generation by cosh-Gaussian laser beams in axially magnetized collisional plasma under non-relativistic ponderomotive regime. Laser Part. Beams **36**, 236–245 (2018). https://doi.org/10.1017/s0263034618000216

Yoshii, J., Lai, C.H., Katsouleas, T., Joshi, C., Mori, W.B.: Radiation from cerenkov wakes in a magnetized plasma. Phys. Rev. Lett. **79**, 4194–4197 (1997). https://doi.org/10.1103/PhysRevLett.79.4194